Applied Catalysis B: Environmental 166–167 (2015) 366–373

Contents lists available at ScienceDirect

Applied Catalysis B: Environmental

journal homepage: www.elsevier.com/locate/apcatb

Visible light photoactivity enhancement via CuTCPP hybridized g-C_3N_4 nanocomposite

Daimei Chen[a,*], Kewei Wang[a,b], Wangzhi Hong[a,b], Ruilong Zong[b], Wenqing Yao[b], Yongfa Zhu[b,*]

[a] Beijing Key Laboratory of Materials Utilization of Nonmetallic Minerals and Solid Wastes, National Laboratory of Mineral Materials, School of Materials Sciences and Technology, China University of Geosciences, Beijing 100083, China
[b] Department of Chemistry, Tsinghua University, Beijing, 100084, PR China

ARTICLE INFO

Article history:
Received 5 October 2014
Received in revised form
21 November 2014
Accepted 24 November 2014
Available online 29 November 2014

Keyword:
Photocatalysis
g-C_3N_4
Sensitization
Porphyrin

ABSTRACT

Cu (II) meso-Tetra (4-carboxyphenyl) porphyrin (CuTCPP) hybridized g-C_3N_4 (CuTCPP/g-C_3N_4) composites have been facilely synthesized through the ethanol dispersion method. CuTCPP molecules as a sensitizer could easily assemble on the surface of g-C_3N_4 nanosheets mainly through π–π stacking interaction. The CuTCPP/g-C_3N_4 composites show much higher photocatalytic activity for phenol degradation than pure g-C_3N_4 under visible light irradiation. The optimum photocatatlytic activity of the CuTCPP/g-C_3N_4 composites with weight ratio of CuTCPP at 0.75% is almost 2.2 times as high as that of pure g-C_3N_4 under the visible light. The enhancement of the visible light photocatalytic activity comes from the efficient electrons transfer from photoexcited CuTCPP molecules to g-C_3N_4 sheets and more efficiently visible-light harvesting due to the CuTCPP sensitization. Both the holes and $\cdot O^{2-}$ are main oxidative species of CuTCPP/g-C_3N_4 for phenol degradation under visible light irradiation. Finally, the possible charge transfer mechanism of enhanced visible light photocatalytic activity was proposed.

1. Introduction

Graphite-like carbon nitride (g-C_3N_4), a metal-free polymer semiconductor, has attracted plenty of attention due to its potential application in solar energy conversion, photosynthesis, electrocatalysis, bioimaging and biomedical application [1–4]. Since Wang et al. firstly reported that the polymeric g-C_3N_4 shows superior H_2 or O_2 evolution activities via water splitting under visible light irradiation, it is considered as an especially promising photocatalyst for hydrogen gas production and organic pollutants degradation using solar energy due to its simple fabrication, low-cost and high stability under light irradiation in solution with pH = 0–14 [5,6]. However, the bandgap of g-C_3N_4 is still as large as 2.7 eV with an absorption edge just at 450 nm, which largely restricts the visible-light utilization efficiency. In addition, the high degree of recombination between photoinduced electrons and holes also blocks its practical application. To overcome these problems, many methods have been proposed to improve the photocatalytic performance of g-C_3N_4, for example, by doping nonmetallic element [7], and coupling g-C_3N_4 with metals [8], organic semiconductors [9,10], graphene [11,12], activated by organic dyes [13].

Among the various strategies for visible-light harvesting, dye sensitization is an efficient and widely used route to extend the spectral response region of wide-band-gap semiconductors [14–16]. Many dye sensitized photocatalysts have been developed for H_2 production, such as sensitized semiconductors [17,18], sensitized multiwall carbon nanotubes [19] and sensitized reduced graphene oxide [20]. Obviously, dye sensitization of g-C_3N_4 can also be an efficient way to enhance the utilization efficiency of visible light. Until now, several dyes such as Erythrosin B (ErB), Eosin Y (EY), poly(3-hexylthiophene) (P3HT) and zinc phthalocyanines (ZnPc) were used as sensitizers of g-C_3N_4 to enhance the photocatalytic H_2 production activity with considerable visible light utilization efficiency [13,21–23].

Porphyrins as light harvesting materials play an important role in photosynthesis. As they possess good chromophore activities over the solar spectrum and good electron donating properties due to their large p-electron systems, porphyrin compounds have been widely regarded as excellent photosensitizers for photocatalysts. For example, the metalloporphyrin-modified TiO_2 system has been reported for the photocatalytic degradation of various kinds of organic pollutants in water under visible light irradiation [24–26]. In generally, metalloporphyrin modified photocatalysts

* Corresponding authors. Tel.: +86 10 82332274; fax: +86 10 82322974.
E-mail addresses: chendaimei@cugb.edu.cn (D. Chen), zhuyf@tsinghua.edu.cn (Y. Zhu).

http://dx.doi.org/10.1016/j.apcatb.2014.11.050
0926-3373/

were prepared by covalent interaction between the different functional groups (—COOH, —OH, etc.) in the periphery of the porphyrin ring and the surface of photocatalysts. It is widely accepted that the covalent bands can form channels, which can enhance the electron transfer between porphyrins and photocatalysts, and further lead to the delocalization of p* orbits of porphyrins [25]. However, the amount of porphyrins absorbed on the surface of the photocatlaysts is limited because most of porphyrins are difficult to covalently interact with photocatlaysts. Zhu et al. prepared porphyrin uncovalently functionalized reduced graphene oxide (RGO) nanocomposite by immobilizing porphyrin on RGO nanosheets via π–π stacking interactions. Porphyrin moiety in the nanocomposite acts as a photosensitizer and harvesting irradiation light. This composite shows remarkable enhanced photocatalytic activity under UV–vis light irradiation due to the fast electrons transfer from photoexcited porphyrin molecules to RGO sheets [27,28]. Considering the g-C_3N_4 has analogue structure with RGO (planar layers with π electron conjugation), it is expected to interact strongly with porphyrins through electrostatic interaction, π–π stacking, or hydrogen bonding. However, to the best our knowledge, there are no studies about the sensitization of g-C_3N_4 with porphyrin, especially the using the dye sensitized g-C_3N_4 for the organic containment degradation. Therefore, a systemic investigation of dye sensitized g-C_3N_4 and the oxidation mechanic of the dye sensitized g-C_3N_4 for the photodegradation needs further studied.

In our paper, we reported the preparation, characterization, and photocatalysis of CuTCPP/g-C_3N_4 composites. Choosing CuTCPP as a sensitizer to hybridize with g-C_3N_4 is not only due to that porphyrin can easily hybridize with g-C_3N_4 through strong π–π stacking interactions, but also due to its nice locally conjugated aromatic structure, as well as its remarkable chemical and thermal stability benefitting for photocatalytic reactions. The optical absorption of g-C_3N_4 (<460 nm) can be greatly extended into longer wavelength of visible light region (450–600 nm) by spectral sensitization with porphyrin. This sensitization photocatalyst shows a high activity for phenol degradation under visible light irradiation because the photogenerated electrons of the excited porphyrin can transfer to g-C_3N_4 efficiently. The present results show the promising application of porphyrin derivatives in a photocatalytic organic degradation system for more efficiently utilizing solar radiation.

2. Experimental

2.1. Material

Dicyandiamide ($C_2H_4N_4$) was purchased from Sinopharm Chemical Reagent Corp, P. R. China. Cu (II) meso-Tetra (4-carboxyphenyl) porphine (CuTCPP, $C_{48}H_{28}CuN_4O_8$) was supported by J&K Scientific Ltd. All other reagents used in this research were analytically pure and used without further purification.

2.2. Sample preparation

2.2.1. Synthesis of g-C_3N_4

Polycondensation of dicyandiamide was employed to obtain g-C_3N_4 according to Ref [29]. Typically, 15 g of dicyandiamide was put in a Muffle Furnace and heated to 550 °C for 4 h to complete the reaction. Finally, the yellow products were collected and ground into powder in an agate mortar.

2.2.2. Synthesis of CuTCPP/g-C_3N_4 composite photocatalyst

The CuTCPP/g-C_3N_4 photocatalysts were prepared by liquid ultrasonic route in ethanol. Firstly, 0.5 g g-C_3N_4 was added into ethanol and then was placed in an ultrasonic bath for an hour to completely disperse the g-C_3N_4. The CuTCPP ethanol solution (0.1 mg mL^{-1}) was added into the above solution and sonicated for an hour. Then the resulting suspension was continually stirred in a fume hood at 60 °C for a night. After completely volatilization of the ethanol, the samples were dried at 100 °C for 8 h. A series of CuTCPP/g-C_3N_4 photocatalysts with the different mass ratios of CuTCPP were prepared by this method, which were denoted as *X*%CuTCPP/g-C_3N_4, where *X* represents the weight ratios of CuTCPP in total (*X*% = 0.1%, 0.25%, 0.5%, 0.75%, 0.8%, 0.9%, 1%, 2%).

2.3. Characterization

The crystallinity of the as-prepared sample was characterized by X-ray diffraction (XRD) on Bruker D8 Advance X-ray diffractometer at room temperature. Morphologies and structures of the prepared samples were further examined with a HITACHI HT770 transmission electron microscopy (TEM) operated at an accelerating voltage of 100 kV. The UV–vis diffuse reflectance spectra (DRS) of the samples were carried out on a Hitachi U-3010 UV–vis spectrophotometer using $BaSO_4$ as the reference. Fourier transform infrared (FTIR) spectra were carried on a Bruker spectrometer in the frequency range of 4000–600 cm^{-1} with a resolution of 1 cm^{-1}. Electrochemical and photoelectrochemical measurements were performed in three-electrode quartz cells with a 0.1 M Na_2SO_4 electrolyte solution. Platinum wire was used as the counter electrode, and saturated calomel electrodes (SCE) were used as the reference electrodes, respectively. The as-prepared photocatalyst film electrodes on ITO served as the working electrode. The photocurrents were measured on an electrochemical system (CHI-660B, China). Electrochemical impedance spectra (EIS) were measured at 0.0 V. A sinusoidal ac perturbation of 5 mV was applied to the electrode over the frequency range of 0.05–105 Hz. Photoluminescence spectra (PL) of the samples were obtained at room temperature excited by incident light of 375 nm using a HORIBA Aqualog Fluorescence Spectrometer.

2.4. Photodegradation experiment

The photocatalytic activities of the as-prepared samples were evaluated by the decomposition of phenol under visible light irradiation. Visible light source was obtained by a 500 W Xe lamp with different wavelengths (420 nm, 450 nm, 470 nm, 490 nm, 510 nm, 550 nm) cutoff filter and, and the average light intensity was 35 mW/cm^2. 25 mg photocatalyst was added into prepared 50 ml 5 ppm phenol solution. Before the light irradiation, the suspensions were firstly ultrasonic dispersed in dark for 15 min, then magnetically stirred for 120 min to reach the adsorption–desorption equilibrium. At given time intervals, 2.8 ml aliquots were sampled and filtered with a micropore membrane. Synchronously, the filtrates of phenol solutions at different conditions were analyzed by recording variations of the phenol peak area. HPLC was adopted to detect phenol concentration and its degradation products distribution. Methanol and water (volume ratio: 60/40) were mobile phase, the elution time was 7 min, the flow rate was 1 ml/min, determine wavelength was 270 nm and chromatographic column was a Venusil XBP-C_{18} (3.9 × 200, Agela Technologies Inc.) column. Before the analysis, the samples were filtered through Millipore discs of 0.45 μm to protect the chromatographic column.

3. Results and discussion

3.1. Morphology and Structure of CuTCPP hybridized g-C_3N_4 photocatalysts

Experimentally, the formation of CuTCPP hybridized g-C_3N_4 structure was involved involves a two-steps process (Scheme 1). First, g-C_3N_4 is exfoliated into sheet structures through an ultrasonic method in ethanol solvent. Secondly, the CuTCPP ethanol solution (0.1 mg mL^{-1}) was added into the above solution and

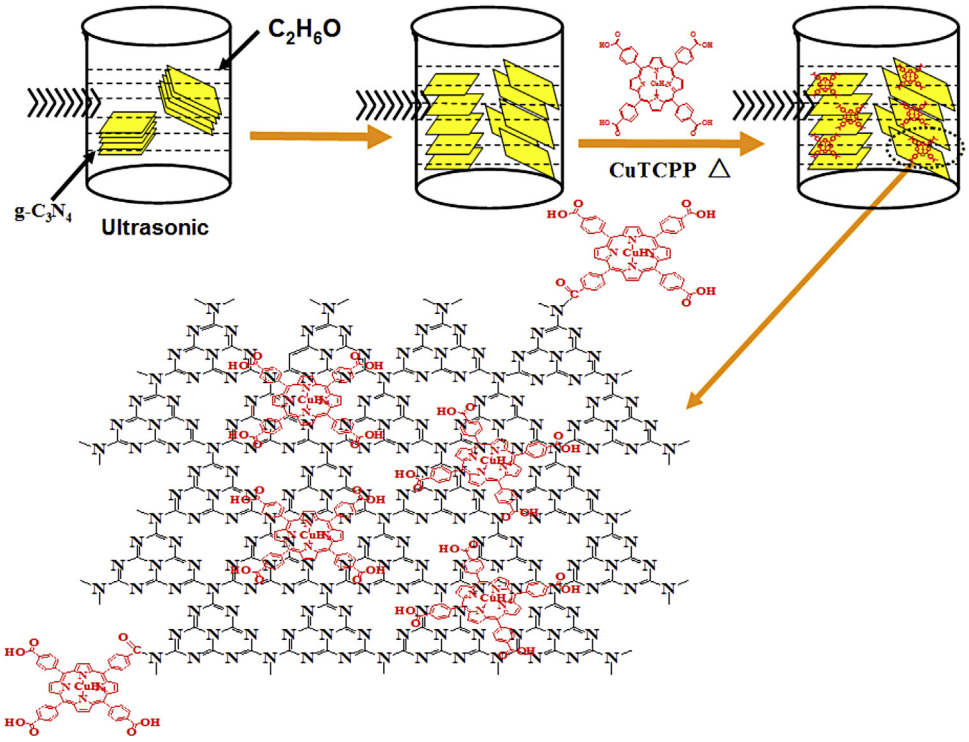

Scheme 1. Schematic illustration of the preparation of the CuTCPP hybridized g-C_3N_4 composites.

bath-sonicated for an hour. Consequently, the CuTCPP molecules will spontaneously coat on the surface of g-C_3N_4 nanosheets through the intermolecular interactions, such as electrostatic interaction and π–π stacking interaction, resulting in a CuTCPP/g-C_3N_4 nanohybrid composite. It is well-known that porphyrin molecules, which have a two-dimensional 18-π-electron aromatic structure, could interact with g-C_3N_4 through π–π stacking. Meanwhile because the functional groups–COOH in the periphery of the CuTCPP ring might interact with the groups —NH_2 on the edge of the g-C_3N_4, the CuTCPP and g-C_3N_4 molecules can also be covalently bonded together by an amide bond. Therefore, both the uncovalently and covalently interactions facilitate the formation of the CuTCPP/g-C_3N_4 hybrid nanocomposite. However, owing to the small amount of the groups —NH_2 on the edge of the g-C_3N_4, the covalent interaction between the CuTCPP and g-C_3N_4 molecules might be very little. So, it can be deduced that the hybridization effect between the CuTCPP and g-C_3N_4 molecules might mainly come from the noncovalent interaction. The great advantage of the strategy of noncovalent interaction is that it can combine the unique properties of the CuTCPP and g-C_3N_4, while it does not disturb the physical properties of both moieties [30].

Fig. 1 shows transmission electron microscopy (TEM) images of pure g-C_3N_4, CuTCPP and 0.75%CuTCPP/g-C_3N_4. Most of irregular and large plates of g-C_3N_4 are observed in Fig. 1a and b. In the image of CuTCPP (Fig. 1 c and d), a lot of small rodlike structure materials can be observed which might be the CuTCPP molecules aggregations. The average size of CuTCPP molecules aggregations is about 50 × 200 nm. For the 0.75%CuTCPP/g-C_3N_4 composite (Fig. 1e and f), there are many large plates of g-C_3N_4, while no CuTCPP aggregation can be found in the TEM image. Meanwhile, compared with pure g-C_3N_4, the agglomeration of CuTCPP/g-C_3N_4 composite becomes more serious. These observations demonstrate that CuTCPP molecules might be well dispersed and attached on g-C_3N_4 plates.

To identify the change of phase structures before and after hybridization, the XRD patterns of the as-prepared CuTCPP/g-C_3N_4 composites, as well as pure g-C_3N_4 and CuTCPP as shown in Figure S1. The g-C_3N_4 sample has a characteristic peak at 27.4°, which can be indexed as the (0 0 2) diffraction plane. And it is can be seen that the crystal phase of g-C_3N_4 did not change with increasing CuTCPP content. There was no crystalline CuTCPP in the CuTCPP/g-C_3N_4 photocatalysts. This fact might be that the loading amount of CuTCPP is too low to detect, and it can also be inferred that CuTCPP molecules dispersed uniformly on the surface of g-C_3N_4, which exhibits a short-range order of CuTCPP molecules arrangement.

The FT-IR spectra of pure g-C_3N_4, pure CuTCPP and a series of CuTCPP/g-C_3N_4 photocatalysts are shown in Fig. 2. In the FT-IR spectrum of g-C_3N_4, the peak at 1637 cm^{-1} is attributable to the C=N stretching vibration modes, while the peaks at 1243 cm^{-1}, 1320 cm^{-1} and 1403 cm^{-1} are due to the aromatic C—N stretching [31–33]. The peak at 808 cm^{-1} is related to the s-triazine ring modes [32]. These peaks are present in the all CuTCPP/g-C_3N_4 composites, suggesting that no structural change of g-C_3N_4 occurs. It can be seen that there was no characteristic peaks of CuTCPP in the CuTCPP/g-C_3N_4 photocatalysts at the low CuTCPP loadings (<2%). When the loading amount of CuTCPP is more than 10%, the main characteristic peaks of CuTCPP molecules can be observed clearly, indicating that the CuTCPP molecules might homogenously immobilized on the surface of the g-C_3N_4 nanosheets and successfully hybridized with g-C_3N_4. However, the characteristic stretching and stretching band of the amide group formed between the CuTCPP and g-C_3N_4 molecules, which are reported to occur at 1640 and 1260, respectively, can not be found in the FT-IR spectra of CuTCPP/g-C_3N_4 composite. The likely reason might be that these peaks are too small to be overlapped by the peaks of g-C_3N_4. This further confirms that the hybridization effect between the CuTCPP and g-C_3N_4 molecules might mainly come from the noncovalent interaction.

3.2. *Photocatalytic activity and photocurrent of CuTCPP hybridized g-C_3N_4 composite photocatalysts*

The photocatalytic performance was mainly evaluated by degradation of phenol, a hazardous pollutant for water as well as a common model to test the photodegradation activity. As shown in Fig. 3a, significant differences in the catalytic behaviors were

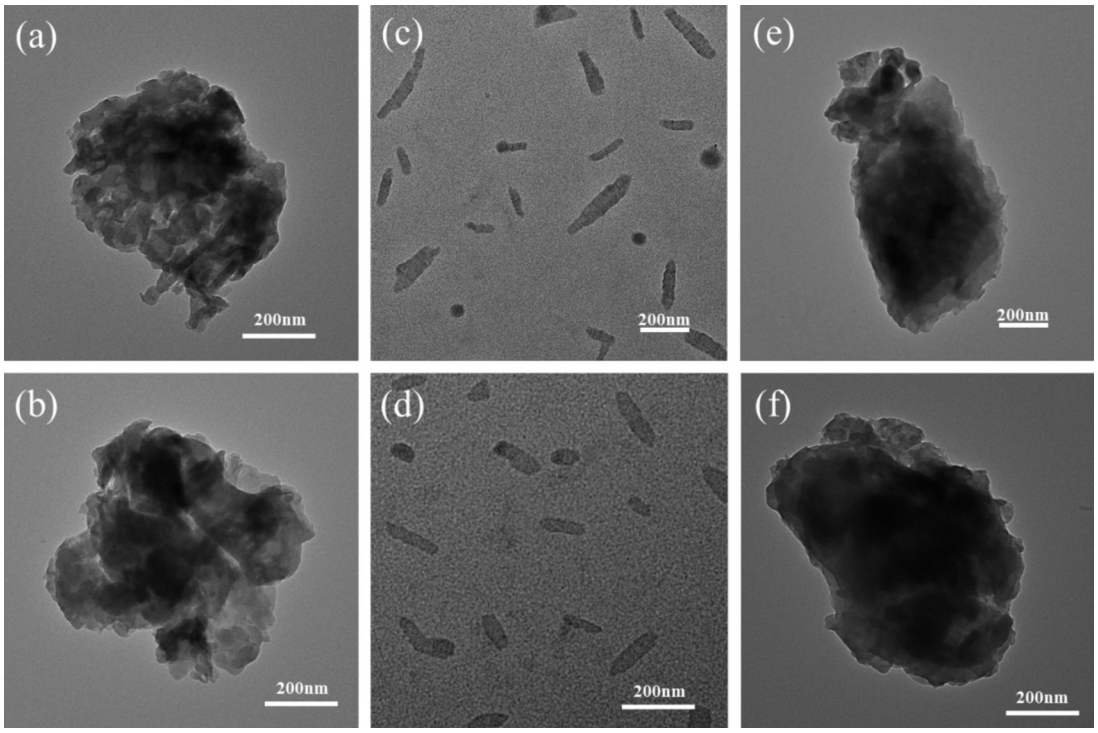

Fig. 1. TEM images of (a, b) pure g-C_3N_4, (c, d) pure CuTCPP, (e, f) 0.75%CuTCPP/g-C_3N_4.

observed, and the photodegradation process was fit to pseudo-first-order kinetics in which the value of rate constant k is equal to the corresponding slope of the fitting line. The blank test confirms that phenol is only slightly degraded in the absence of catalysis, indicating that the photolysis effects can be ignored. Under visible light irradiation, the apparent rate constant k of pure CuTCPP is 0.0012 h^{-1}, suggesting that the CuTCPP itself hardly has any the visible light activity. All of the CuTCPP/g-C_3N_4 composites exhibited higher photocatalytic activity than the single CuTCPP and g-C_3N_4 under visible light irradiation. The photocatalyst activity of CuTCPP/g-C_3N_4 was enhanced gradually with the increasing proportion of CuTCPP and reaches the optimum activity when the loading amount of CuTCPP is up to 0.75 wt.%. However, as the proportion of CuTCPP further increases, the degradation rate decreases gradually. The apparent k of 0.75% CuTCPP/g-C_3N_4 sample is 0.024 h^{-1}, which was about 2.18 times as high as that of pure g-C_3N_4 sample (0.011 h^{-1}).

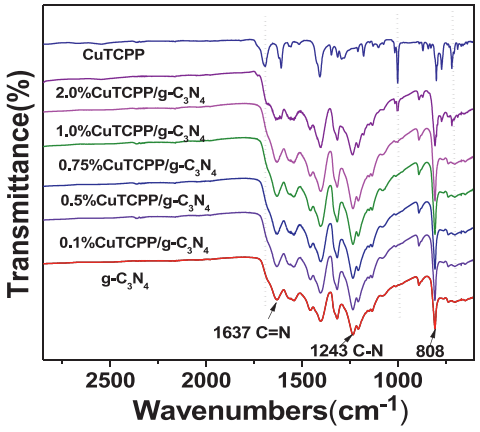

Fig. 2. FT-IR spectra of g-C_3N_4, CuTCPP and CuTCPP/g-C_3N_4 photocatalysts.

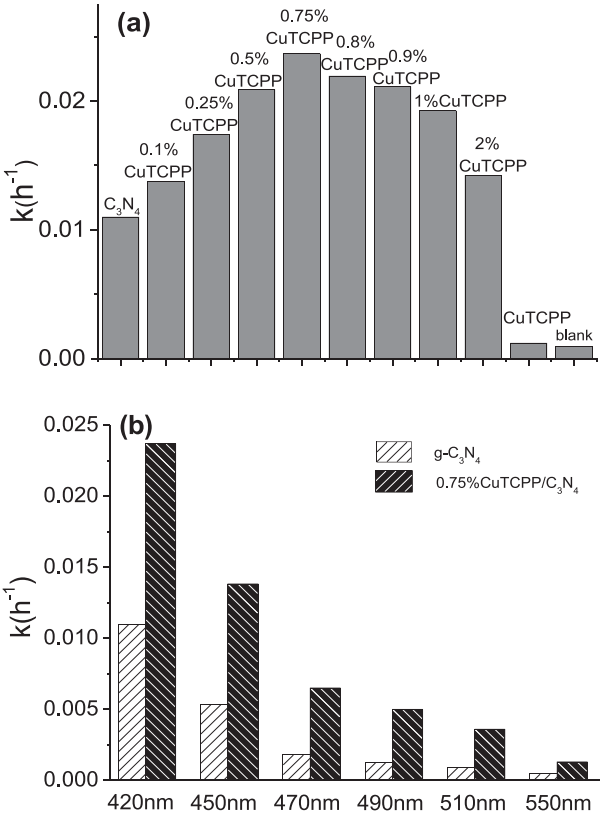

Fig. 3. Apparent rate constants for the photocatalytic degradation of phenol (a) over g-C_3N_4, CuTCPP and CuTCPP/g-C_3N_4 photocatalysts under visible light irradiation ($\lambda > 420$ nm); (b) over g-C_3N_4 and 0.75%CuTCPP/g-C_3N_4 photocatalysts under different wavelength light irradiation.

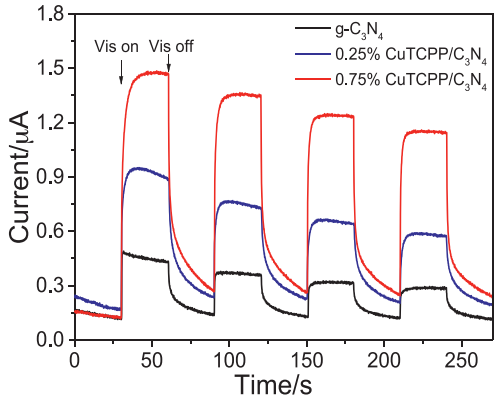

Fig. 4. The transient photocurrent density responses of pure g-C_3N_4, 0.25%CuTCPP/g-C_3N_4 and 0.75%CuTCPP/g-C_3N_4 samples electrodes with light on/off cycles under visible light irradiation (λ > 420 nm).

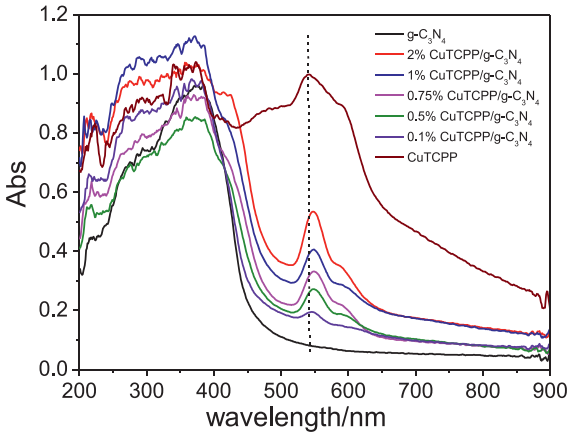

Fig. 5. UV–vis diffuse reflection spectra of g-C_3N_4, CuTCPP and CuTCPP/g-C_3N_4 photocatalysts.

The phenol photodegradation intermediates are investigated by chromatograms of phenol before and after photocatalytic degradation for 10 h monitored at 275 nm (Fig. S3). The peak at 5.3 min can be identified as that of phenol. The peak at 3.2, 2.8 and 2.1 min are oxidized intermediates, which might be hydroquinol (HQ), maleic acid (MA) and the lower fatty acid, respectively [34,35]. As the reaction proceeded, the peak of phenol became lower, whereas the peaks of the intermediate species increased gradually. The higher intensity of intermediates by 0.75%CuTCPP/g-C_3N_4 than pure g-C_3N_4 indicates that the degradation ability of 0.75%CuTCPP/g-C_3N_4 is remarkably enhanced and the intermediates could be further degraded by ring cleavage and finally subjected to complete degradation to CO_2 and H_2O.

In order to clearly elucidate the extended photoresponse and enhanced photocatalytic activity of CuTCPP/g-C_3N_4 photocatalyst in longer wavelength visible regions, the wavelength dependence of photocatalytic activity for phenol degradation over sensitization photocatalyst investigated in the range of 420–550 nm using various band pass filters (λ = 420, 450, 470, 490, 510 and 550 nm). Fig. 3b compared the value of rate constants *k* of pure g-C_3N_4 and 0.75%CuTCPP/g-C_3N_4 composite under different ranges of the wavelength. The overall enhanced photocatalytic activity for phenol degradation is observed on 0.75%CuTCPP/g-C_3N_4 across the whole of its absorption spectrum. This wavelength-independent enhancement indicates there may be some interactions between CuTCPP and g-C_3N_4 that plays an important role in improving the photocatalytic activity. It can be seen that the photocatalytic activity decrease with increasing wavelengths. With the increase the wavelengths from 420 nm to 550 nm, the rate constants of g-C_3N_4 decrease from 0.01098 to 0.00045 h^{-1}, and those of 0.75%CuTCPP/g-C_3N_4 decrease from 0.02368 to 0.00128 h^{-1}. This fact is ascribed to the decrease of the available photon energy with the increase of wavelengths, and further confirms that CuTCPP as sensitizer can extend photoresponse of g-C_3N_4 and improve utilization efficiency of visible light.

The photocurrent responses of 0.75%CuTCPP/g-C_3N_4, 0.25%CuTCPP/g-C_3N_4 and pure g-C_3N_4 after deposition on ITO electrodes under visible light (λ > 420 nm), are shown in Fig. 4. The transient photocurrent responses of a photocatalysis may directly correlate with the recombination efficiency of the photogenerated carriers [36–38]. It is obvious to observe that the photocurrent over CuTCPP/g-C_3N_4 is greatly improved, and the optimum 0.75%CuTCPP/g-C_3N_4 sample electrode is about 3.5 times as high as that of the pure g-C_3N_4 electrode. The enhanced photocurrent over CuTCPP/g-C_3N_4 sample implies more efficient separation of the photoinduced electron-hole pairs and longer lifetime of the photogenerated charge carriers than that of pure g-C_3N_4, which is beneficial for its enhanced photocatalytic activity.

3.3. Mechanism of photocatalytic activity enhancement

The absorption range of light plays an important role in the photocatalysis, especially for the visible light photodegradation of contaminants. Fig. 5 shows the UV–vis diffuse reflectance spectroscopy (DRS) of CuTCPP/g-C_3N_4 composites, as well as pure g-C_3N_4 and CuTCPP. The pure g-C_3N_4 exhibits a fundamental absorption edge at 450 nm, corresponding to the band gap of 2.7 eV. The pure CuTCPP sample has strong absorption in visible region (400–700 nm) and a strongest absorption intensity peak at 538 nm, which identified as the Q band of porphyrin. As increasing the loading amount of CuTCPP in the CuTCPP/g-C_3N_4 composites, the absorption intensities of the composites are enhanced and the absorption edges also show a slight red shift. The CuTCPP/g-C_3N_4 composite samples show hybrid absorption features of g-C_3N_4 and CuTCPP, which allows for more efficient utilization of the solar spectrum to create photogenerated electrons and holes. Fig. S2 (see the Supporting Information) shows that the Q bands centered at 545 nm attributed to the Q band of CuTCPP adsorbed on the g-C_3N_4 nanosheet is founded to have a slight red shift of 7 nm as compared to its absorption in methanol at 538 nm, suggesting that π–π stacking interactions between the individual components in the CuTCPP/g-C_3N_4 nanocomposite [39,40]. A significant broadening of the Soret band peak can also be observed in the absorption of CuTCPP solid and CuTCPP absorbed on the g-C_3N_4 as compared to the absorption spectra of in methanol. This phenomenon is due to the dye aggregations on the solid substrates [41].

It is well known that phase structure, BET surface area, and separation efficiency of photogenerated charges are the key factor to influent the photocatalytic activity. As can be seen from the XRD spectra, the crystal phase structure of g-C_3N_4 does not changed after the hybridization of the g-C_3N_4. The BET surface area of g-C_3N_4 is 8.2 m^2/g, and those of 0.1%CuTCPP/g-C_3N_4, 0.25%CuTCPP/g-C_3N_4, 0.75%CuTCPP/g-C_3N_4, 0.9%CuTCPP/g-C_3N_4, 1.0%CuTCPP/g-C_3N_4, and 2.0%CuTCPP/g-C_3N_4 are 10.1 m^2/g, 9.8 m^2/g, 7.3 m^2/g, 7.2 m^2/g, 7.0 m^2/g, 6.3 m^2/g, respectively. This fact shows that the hybridization with CuTCPP has a little effect in BET surface area of g-C_3N_4. Furthermore, the adsorption experiment shows that adsorption abilities of the g-C_3N_4 and CuTCPP/g-C_3N_4 nanocomposites toward phenol are almost same. Therefore, the important reason for the enhancement of photocatalytic activity on CuTCPP/g-C_3N_4 nanocomposite is due to the effective separation of the photogenerated

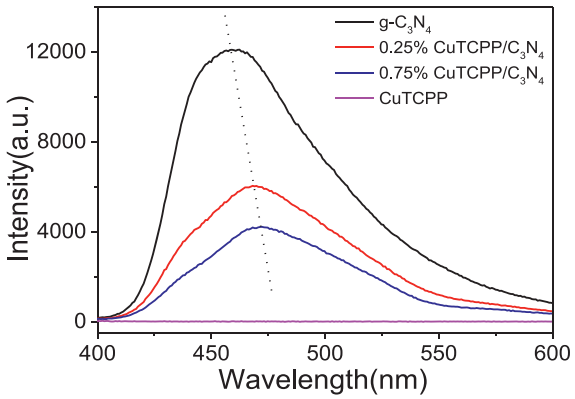

Fig. 6. Photoluminescence spectra of pure g-C_3N_4, pure CuTCPP, 0.25%CuTCPP/g-C_3N_4 and 0.75%CuTCPP/g-C_3N_4 photocatalysts.

electron-hole pairs induced by the energy level match between g-C_3N_4 and CuTCPP.

Photoluminescence (PL) technique can be also employed to investigate the migration, transfer and recombination processes of photogenerated electron–hole pairs in semiconductors [42]. Fig. 6 presents the photoluminescence spectra for pure g-C_3N_4, 0.75%CuTCPP/g-C_3N_4, 0.25%CuTCPP/g-C_3N_4 and pure CuTCPP at an excitation wavelength of 375 nm. Pure g-C_3N_4 shows a strong, wide peak in the PL spectrum, while pure CuTCPP has no PL signal response at the excitation wavelength. The PL peak of the CuTCPP/g-C_3N_4 composites decrease remarkably compared with the pure g-C_3N_4, indicating the recombination of electrons and holes is hindered greatly. Moreover, in comparison with pure g-C_3N_4, the intensity of the PL signal for the CuTCPP/g-C_3N_4 composite shows an obvious red-shift, which further indicates that there may be some interactions between CuTCPP and g-C_3N_4. Therefore it can be concluded that CuTCPP have been successfully hybridized with g-C_3N_4 and the faster separation of photogenerated charges is direct reason for the enhanced photocatalytic activities of CuTCPP/g-C_3N_4 composites.

To reveal the photocatalytic mechanism further, the interface charge separation efficiency is investigated by the typical electrochemical impedance spectra (presented as Nyquist plots). Fig. 7 shows electrochemical impedance spectra (EIS) Nyquist plots of 0.75%CuTCPP/g-C_3N_4, 0.25%CuTCPP/g-C_3N_4 and pure g-C_3N_4 electrodes before and after visible light irradiation ($\lambda > 420$ nm). The arc radius on the EIS Nyquist plot can reflect the reaction rate on the surface of the electrode. This smaller arc radius implies a more effective separation of photogenerated electron–hole pairs

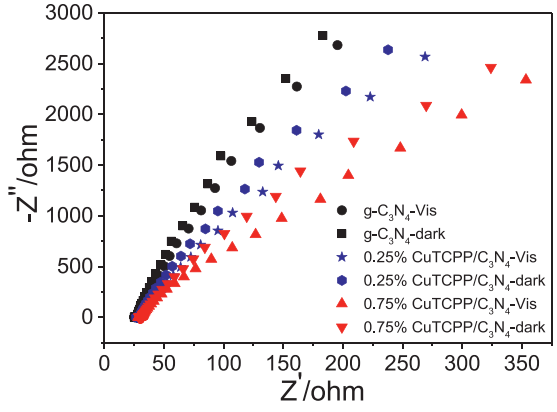

Fig. 7. Nyquist plots for pure g-C_3N_4, 0.25%CuTCPP/g-C_3N_4 and 0.75%CuTCPP/g-C_3N_4 in aqueous solution in the dark and under visible light illumination ($\lambda > 420$ nm) [Na_2SO_4 = 0.1 M].

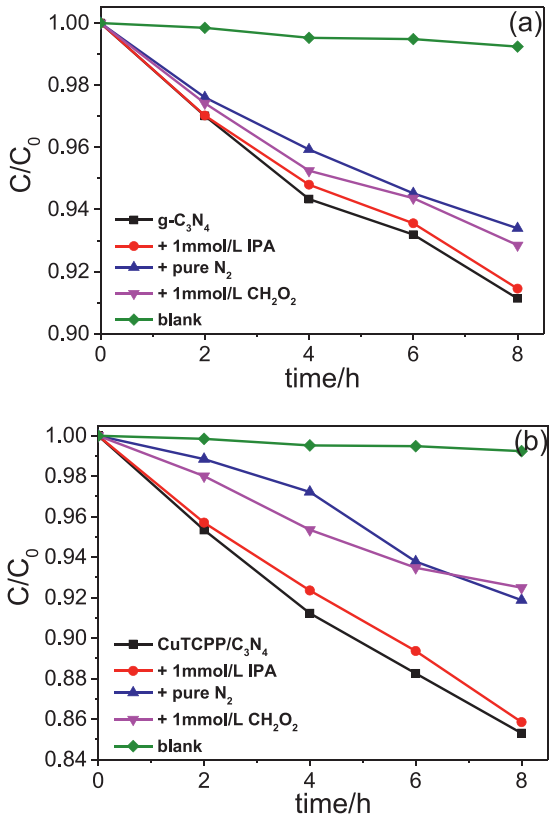

Fig. 8. The plots of photogenerated carriers trapping in the system of photodegradation of MB by (a) pure g-C_3N_4 and (b) 0.75%CuTCPP/g-C_3N_4, under visible light irradiation ($\lambda > 420$ nm), respectively.

and a higher efficiency of charge immigration across the electrode/electrolyte interface [43]. The arc radii of CuTCPP/g-C_3N_4 samples electrode are smaller than that of pure g-C_3N_4 electrode, suggesting that CuTCPP/g-C_3N_4 composite structure can make the separation and immigration of photogenerated electron-hole pairs more efficient, which is in good accordance with the result of the photocurrent measurement.

It is important to detect main oxidative species in the photocatalytic process for elucidating the photocatalytic mechanism. The main oxidative species in photocatalytic process are detected through the trapping experiments of radicals using IPA as hydroxyl radical scavenger [44] and CH_2O_2 as holes radical scavenger [45], and purging N_2 as $\cdot O^{2-}$ scavenger[46], respectively. As shown in Fig. 8a, the photocatalytic degradation of phenol with g-C_3N_4 hardly has any change by the addition of IPA in the reaction system, while has a remarkably decrease by the addition of CH_2O_2 and purging N_2 gas, indicating that both $\cdot O^{2-}$ and photogenerated holes might have the effect on the phenol degradation in the pure g-C_3N_4 system. For CuTCPP/g-C_3N_4 composite, the change tendency is same with the g-C_3N_4. The photocatalytic activity is greatly suppressed by the addition of a scavenger for holes (CH_2O_2) and by N_2 gas in the reaction system (Fig. 8b). While the addition of IPA only causes a slight change in the photodegradation of phenol. This fact indicates that both $\cdot O^{2-}$ and photogenerated holes are main oxidative species of CuTCPP/g-C_3N_4 for phenol degradation under visible light irradiation. However, compared with pure g-C_3N_4, the straight slopes of CuTCPP/g-C_3N_4 samples with same addition of CH_2O_2 and N_2 decline more obviously, indicating that there may exist more holes and $\cdot O^{2-}$ in CuTCPP/g-C_3N_4 system than in pure g-C_3N_4 system due to the effective separation of photogenerated electron–hole pairs.

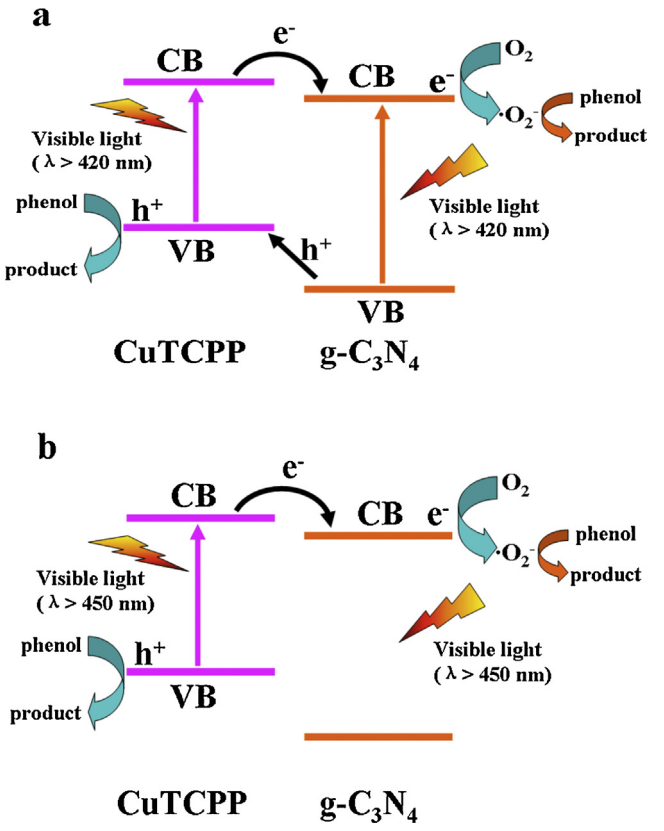

Fig. 9. Schematic drawing illustrating the mechanism of charge separation and photocatalytic activity of the CuTCPP/g-C_3N_4 photocatalyst under visible light irradiation (a) λ > 420 nm; (b) λ > 450 nm.

On the base of the above information, a possible mechanism for the phenol photodegradation using the CuTCPP hybridized g-C_3N_4 photocatalyst is proposed as illustrated in Fig. 9. Both the g-C_3N_4 and CuTCPP can be excited by visible light (λ > 420 nm) and produce photogenerated electrons and holes (Fig. 9 a). Since the conduction band (CB) position of CuTCPP is lower than that of g-C_3N_4, the photoinduced electrons on the CB of CuTCPP can directly transfer to the CB of g-C_3N_4. Consequently, the photoinduced electrons in CB of g-C_3N_4 are good reducing agents that could capture the adsorbed O_2 onto the composite catalyst surface and reduce it to $\cdot O^{2-}$. Subsequently, phenol molecules can be degraded by oxidation reaction with $\cdot O^{2-}$. Meanwhile, the corresponding valence band (VB) position of g-C_3N_4 is lower than that of CuTCPP, the photogenerated holes on the VB of g-C_3N_4 can spontaneously immigrate to the VB of CuTCPP. The holes on VB of CuTCPP can directly degrade the organic compounds under visible light irradiation. Therefore, an effective charge separation can be achieved due to the well-matched overlapping band structures and closely contacted interfaces between CuTCPP and g-C_3N_4. This fact reduces the probability of charges recombination, resulting in enhanced photocatalytic activity under visible light irradiation.

In addition, when the wavelength is larger than 450 nm (Fig. 9 b), g-C_3N_4 cannot be excited. CuTCPP can still be excited due to its strong absorption in visible region (400–700 nm), and produce photogenerated electrons and holes. Consequently the photoinduced electrons on the CB of CuTCPP can transfer to the CB of g-C_3N_4, and react with adsorbed O_2 on the surface of g-C_3N_4 into $\cdot O^{2-}$. The $\cdot O^2$ can react with H_2O to form ·OH or directly oxidize the organic compound into CO_2 and H_2. Therefore, the sensitization g-C_3N_4 with CuTCPP can lead to an overall enhanced photocatalytic activity across the whole of its absorption spectrum.

4. Conclusion

In this work, we present a simple method to prepare CuTCPP/g-C_3N_4 nanohybrid photocatalyst for the organic compound degradation. Porphyrin can easily hybridize with g-C_3N_4 through strong π–π stacking interactions without much influence on the electronic properties of the g-C_3N_4. Sensitization of g-C_3N_4 with CuTCPP affords a highly efficient photocatalyst for phenol degradation under visible light irradiation. When the CuTCPP content in CuTCPP/g-C_3N_4 composites achieves 0.75%, the photocatalytic activity is up to the maximum, which is almost 2.2 times as high as that of pure g-C_3N_4 under the visible light. Both the holes and $\cdot O^{2-}$ are main oxidative species of CuTCPP/g-C_3N_4 for phenol degradation under visible light irradiation. The enhancement in photocatalytic performance under the visible light irradiation is ascribed to not only the well-matched overlapping band structures, which facilitating the separation and transfer of photogenerated electron–hole pairs, but also the sensitization effect of CuTCPP, which leading to an overall enhanced photocatalytic activity of g-C_3N_4 across the whole its absorption spectrum.

Acknowledgements

This present work is supported by the National Natural Science Foundations of China (Grant No.21106138), the Fundamental Research Funds for the Central Universities (Grant No. 2011YXL062), National High Technology Research and Development Program of China (2012AA062701), Open fund of National Laboratory of Mineral Materials (Grant No. 09A003).

Appendix A. Supplementary data

Supplementary data associated with this article can be found, in the online version, at http://dx.doi.org/10.1016/j.apcatb.2014.11.050.

References

[1] J. Sun, J. Zhang, M. Zhang, M. Antonietti, X. Fu, X. Wang, Nat. Commun. 3 (2012) 1132–1139.
[2] F. Goettmann, A. Thomas, M. Antonietti, Angew. Chem. Int. Ed. 46 (2007) 2717–2720.
[3] Y. Zhang, A. Thomas, M. Antonietti, X. Wang, J. Am. Chem. Soc. 131 (2009) 50–51.
[4] Z.H. Zhang, K. Leinenweber, M. Bauer, L.A.J. Garvie, P.F. McMillan, G.H. Wolf, J. Am. Chem. Soc. 123 (2001) 7788–7796.
[5] G. Liu, P. Niu, C.H. Sun, S.C. Smith, Z.G. Chen, G.Q. Lu, H.M. Cheng, J. Am. Chem. Soc. 132 (2010) 11642–11648.
[6] X.C. Wang, K. Maeda, A. Thomas, K. Takanabe, G. Xin, J.M. Carlsson, K. Domen, M. Antonietti, Nat. Mater. 8 (2009) 76–80.
[7] Y. Wang, J.S. Zhang, X.C. Wang, M. Antonietti, H.R. Li, Angew. Chem. Int. Ed. 49 (2010) 3356–3359.
[8] Y. Di, X.C. Wang, A. Thomas, M. Antonietti, ChemCatChem 2 (2010) 834–838.
[9] G.Z. Liao, S. Chen, X. Quan, H.T. Yu, H.M. Zhao, J. Mater. Chem. 22 (2012) 2721–2726.
[10] H.J. Yan, Y. Huang, Chem. Commun. 47 (2011) 4168–4170.
[11] Q.J. Xiang, J.G. Yu, M. Jaroniec, J. Phys. Chem. C 115 (2011) 7355–7363.
[12] Y.J. Zhang, T. Mori, L. Niu, J.H. Ye, Energ. Environ. Sci. 4 (2011) 4517–4521.
[13] S. Min, G. Lu, J. Phys. Chem. C 116 (2012) 19644–19652.
[14] T. Kamegawa, S. Matsuura, H. Seto, H. Yamashita, Angew. Chem. 125 (2013) 950–953.
[15] M. Latorre-Sánchez, C. Lavorato, M. Puche, V. Fornés, R. Molinari, H. Garcia, Chem. A Eur. J. 18 (2012) 16774–16783.
[16] Y. Park, W. Kim, D. Monllor-Satoca, T. Tachikawa, T. Majima, W. Choi, J. Phys. Chem. Lett. 4 (2013) 189–194.
[17] R. Abe, K. Hara, K. Sayama, K. Domen, H. Arakaw, J. Photochem. Photobiol. A: Chem. 137 (2000) 63–69.
[18] Q.Y. Li, Z.L. Jin, Z.G. Peng, Y.X. Li, S.B. Li, G.X. Lu, J. Phys. Chem. C 111 (2007) 8237–8241.
[19] Q.Y. Li, L. Chen, G.X. Lu, J. Phys. Chem. C 111 (2007) 11494–11499.
[20] S.X. Min, G.X. Lu, J. Phys. Chem. C 115 (2011) 13938–13945.
[21] Y. Wang, J. Hong, W. Zhang, R. Xu, Catal. Sci. Technol. 3 (2013) 1703–1711.
[22] H. Yan, Y. Huang, Chem. Commun. 47 (2011) 4168–4170.
[23] L. Yu, X. Zhang, C. Zhuang, L. Lin, R. Li, T. Peng, Phys. Chem. Chem. Phys. 16 (2014) 4106–4114.

[24] C. Wang, J. Li, G. Mele, G.-M. Yang, F.-X. Zhang, L. Palmisano, G. Vasapollo, Appl. Catal. B: Environ. 89 (2009) 448–454.
[25] D. Chen, D. Yang, J. Geng, J. Zhu, Z. Jiang, Appl. Surf. Sci. 255 (2008) 2879–2884.
[26] W.J. Sun, G. Li, M. Yao, F. Jiang, Zhang, Catal. Commun. 16 (2011) 90–93.
[27] M. Zhu, Z. Li, B. Xiao, Y. Lu, Y. Du, P. Yang, X. Wang, ACS Appl. Mater. Interfaces 5 (2013) 1732–1740.
[28] Y. Chen, Z.-H. Huang, M. Yue, F. Kang, Nanoscale 6 (2014) 978–985.
[29] X. Wang, K. Maeda, A. Thomas, K. Takanabe, G. Xin, J.M. Carlsson, K. Domen, M. Antonietti, Nat. Mater. 8 (2009) 76–80.
[30] V. Georgakilas, M. Otyepka, A.B. Bourlinos, V. Chandra, N. Kim, K.C. Kemp, P. Hobza, R. Zboril, K.S. Kim, Chem. Rev. 112 (2012) 6156–6214.
[31] Y.C. Zhao, D.L. Yu, H.W. Zhou, Y.J. Tian, O. Yanagisawa, J. Mater. Sci. 40 (2005) 2645–2647.
[32] X. Li, J. Zhang, L. Shen, Y. Ma, W. Lei, Q. Cui, G. Zou, Appl. Phys. A 94 (2009) 387–392.
[33] L. Liu, D. Ma, H. Zheng, X. Li, M. Cheng, X. Bao, Micropor. Mesopor. Mater. 110 (2008) 216–222.
[34] L. Liu, H. Liu, Y.P. Zhao, Y. Wang, Y. Duan, G. Gao, M. Ge, W. Chen, Environ. Sci. Technol. 42 (2008) 2342–2348.
[35] Y. Liu, Y. Zhu, J. Xu, X. Bai, R. Zong, Y. Zhu, Appl. Catal. B: Environ. 142–143 (2013) 561–567.
[36] H. Liu, S. Cheng, M. Wu, H. Wu, J. Zhang, W. Li, C. Cao, J. Phys. Chem. A 104 (2000) 7016–7020.
[37] W.H. Leng, Z. Zhang, J.Q. Zhang, C.N. Cao, J. Phys. Chem. B 109 (2005) 15008–15023.
[38] H. Park, W. Choi, J. Phys. Chem. B 107 (2003) 3885–3890.
[39] Y. Xu, L. Zhao, H. Bai, W. Hong, C. Li, G. Shi, J. Am. Chem. Soc. 131 (2009) 13490–13497.
[40] W. Tu, J. Lei, S. Zhang, H. Ju, Chem. A Eur. J. 16 (2010) 10771–10777.
[41] P. Castillero, J.R. Sanchez-Valencia, M. Cano, J.M. Pedrosa, J. Roales, A. Barranco, A.R. Gonzalez-Elipse, ACS Appl. Mater. Interfaces 2 (2010) 712–721.
[42] Y.-S. Xu, W.-D. Zhang, ChemCatChem 5 (2013) 2343–2351.
[43] S.J. Hong, S. Lee, J.S. Jang, J.S. Lee, Energ. Environ. Sci. 4 (2011) 1781–1787.
[44] L.-S. Zhang, K.-H. Wong, H.-Y. Yip, C. Hu, J.C. Yu, C.-Y. Chan, P.-K. Wong, Environ. Sci. Technol. 44 (2010) 1392–1398.
[45] T. Tan, D. Beydoun, R. Amal, J. Photochem. Photobiol. A: Chem. 159 (2003) 273–280.
[46] C. Pan, Y. Zhu, Environ. Sci. Technol. 44 (2010) 5570–5574.